3D Laser Imaging and Sparse Points Grouping for Pavement Crack Detection

Qingquan Li

4S Lab, Shenzhen University
liqq@szu.edu.cn

Dejin Zhang

EE, Hubei Univ. of Tech.
djzhang@whu.edu.cn

Qin Zou

CS, Wuhan University
qzou@whu.edu.cn

Hong Lin

Zoyon Co., Ltd.
honglin@gmail.com

Abstract—Traditional optical imaging has limitations in capturing and representing pavement cracks due to the impact of illumination variations and cast shadows. In this work, laser-imaging techniques are employed to model the pavement surface with dense 3D points, and a sparse points grouping method is proposed to detect cracks from the 3D point clouds. Firstly, an algorithm based on frequency analysis is presented to separate potential cracks from the control profile and material texture of the pavement. Secondly, range images generated from point clouds are partitioned into image patches, and a learning algorithm is used to identify image patches probably containing cracks. Thirdly, the extracted patches are further filtered by checking the consistency of potential crack directions. Finally, edge weights are assigned to crack seed pairs by referring to the Gestalt law, and minimum spanning tree based algorithms are developed to extract the final cracks. Extensive experiments demonstrate the effective of the proposed method.

I. Introduction

The pavement crack is the most common distress on road surface. Automatic crack detection and timely crack repairing are very important to traffic safety and management economy, which promotes the development of crack detection systems and algorithms [1]–[7]. Traditional optic-imaging-based crack detection methods often have limitations since the quality of optic images can easily be undermined by the illumination variations and cast shadows and the consequent complications would heavily increase the difficulty of pavement crack detection [8]. To overcome the above weakness of using optic imaging, this work models the pavement surface by utilizing a 3D laser imaging technique, and develops new algorithms to detect pavement cracks from dense 3D point clouds.

In the past several years, 3D laser imaging techniques have been widely used in a variety of engineering applications including pavement crack detection [9]–[15], in which line-structure laser scanning techniques were used to produce 3D profile of pavement surface. The 3D laser profiling data reflects the relative change of pavement elevation on pavement cross section. Generally, the fractures in elevation are obviously different between the normal textures caused by pavement particles and the cracks, since the 3D crack's elevations are mostly lower than texture's elevations, and cracks usually have good continuity, directionality and aggregation. The factors that influence data quality in optic imaging such as shadows, ambient light, road surface stains have little impact on the 3D laser imaging case. However, the crack detection based on 3D laser points needs to overcome several key problems:

- Separating particle textures from the profiling data. The pavement textures and pavement cracks can easily be confused as both of them are high frequency signals while showing local fluctuations. The rich texture fluctuation of the pavement will affect the accurate detection of cracks, especially for the cracks with shallow depth.
- Separating the control profile from the profiling data. The control profile of road pavement is formed in road construction, and it can be affected by the pavement macro-deformation such as pothole, which increases the difficulty of accurate pavement control profile extraction. The bias of the extracted control profile will incur less precise localization of cracks.
- Detecting the whole pavement cracks accurately. The cracks in the 3D cross section usually displays its aggregation but poor continuity in shifted depth, which leads to the detected cracks are often in fragments rather than its complete structure.

In this work, based on the frequency analysis of the laser profiling data, we proposed algorithms to separate the pavement textures and control profile from the profiling pavement cross section. After the separation, we transform the laser point cloud into range images, in which we carefully formulate the threshold to preserve the potential cracks while removing the pavement texture. Then, a sparse points grouping method is performed to detect pavement cracks which contains several key steps such as crack sub-block classification, crack blocks filtering and crack seeds grouping. Finally, the proposed crack detection method is validated by extensive evaluations on large real datasets in the experiments.

II. 3D Laser Profiling Data Preprocessing

The asphalt pavement is mainly made up of asphalt concrete, including asphalt material in dark and grain ingredients with different size. Generally, the grain ingredients constitute a uniform textured structure with slight undulation on the pavement surface – *grain texture*, which provides necessary friction forces for the traffic. The road pavement in the absence of pavement distresses commonly holds a relatively uniform shape – *control profile*. Therefore, the road surface profiling by a laser imaging is a compound of the grain texture, road control profile and the distress shape, as illustrated by Fig. 1. It is necessary to decompose these components by data preprocessing.
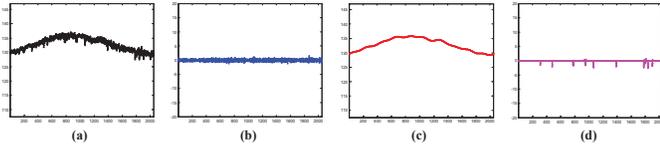
Fig. 1. An illustration of profile decomposition in laser scanning. (a) A profiled pavement surface captured by laser imaging – the real profile. (b) The grain texture. (c) The road's control profile. (d) The profiled cracks.

A. Profile data frequency analysis

In digital signal processing, the fast Fourier transformation (FFT) is often employed to transform the signal from the time-space domain to the frequency domain. The low-frequency component of the signal represents the basic trend of the signal variation, while the high-frequency component represents the relatively sharp signal change. In the space-time domain, the pavement texture, crack and pavement control profile are compound and difficult to perform the accurate extraction and location of the pavement control profile and crack detection. In the frequency domain, the pavement texture and crack correspond to the high frequency part in the spectrum, while the pavement control profile correspond to the low-frequency part. Therefore, the FFT can effectively separate the control profile from the profiling data. Figure 2(a)-(c) show the amplitude and power spectrum of the signal after FFT. As the pavement control profile is a smooth part of the pavement surface, it can be intercepted using the band-pass filter.
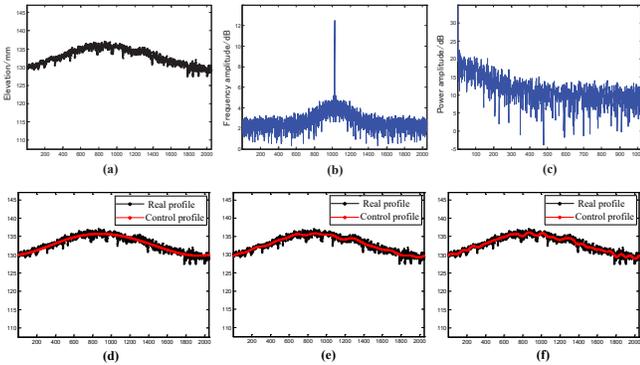

Fig. 2. The top row shows the results produced by FFT, and the bottom row shows the control profiles at different filtering values (F_{s1}). (a) The original profile of a traverse section of the pavement. (b) The amplitude spectrum of the FFT frequency. (c) The power spectrum of the FFT frequency. (d) $F_{s1}=0.003*F_H$. (e) $F_{s1}=0.015*F_H$. (f) $F_{s1}=0.03*F_H$.

B. Control profile calculation

In contrast to the FFT process, the inverse fast Fourier transformation (IFFT) transform the signal from the frequency domain to the space-time domain. The IFFT result based on the low-frequency band power spectrum corresponds to the pavement control profile. The low-frequency signal after filtering ranges from 0 to F_{s1}, and the recovered control profiles are shown in Fig. 2(d)-(f) at three different F_{s1}, respectively. Note that, F_H denotes the maximum band power

of the frequency spectrum. When the filtering frequency F_{s1} = 0.003*F_H, the recovered control profile is so smooth that it deviates from the ground truth control profile, as shown in Fig. 2(d). For F_{s1} = 0.015*F_H, the recovered control profile well represents the shape of road surface, as shown in Fig. 2(e). For F_{s1} = 0.03*F_H, the recovered control profile is too fine to avoid the cracks, as shown in Fig. 2(f). In our work, we empirically set $F_{s1}=0.015*F_H$ to obtain the control profile.

C. Potential crack separation

It is necessary to calculate a threshold value for each cross-section profiling data by analyzing the texture distribution, and obtain the potential cracks by using the threshold value and the pre-computed pavement control profile. The elevation difference between the pavement profile and the control profile can reflect the distribution of the elevations of the texture in each cross section. Let PP_i and CP_i be the elevation values of the ith point on the pavement profile and control profile, respectively, then, the mean difference and the mean squared values of the texture can be calculated by Eq. 1 and Eq. 2,

$$AvgTex = \frac{1}{N} \sum_{i=1}^{N} |PP_i - CP_i|, \tag{1}$$

$$DevTex = [\frac{1}{N} \sum_{i=1}^{N} (|PP_i - CP_i| - AvgTex)^2]^{\frac{1}{2}}, \tag{2}$$

where N represents the total number of sampling points on a single section. The split threshold $\mathcal{T}$ can be calculated by Eq. 3, in which k is the coefficient of threshold ($2 \leqslant k \leqslant 3$). And the potential crack point on the section can be judged by Eq. 4, hence a binary crack map can be obtained to indicate the potential cracks.

$$\mathcal{T} = AvgTex + k * DevTex \tag{3}$$

$$\mathcal{B}_i = \begin{cases} 1, & if \ (PP_i - CP_i) > \mathcal{T} \\ 0, & else \end{cases} \tag{4}$$

III. PAVEMENT CRACK DETECTION

In this section, we introduce our crack detection methods using 3D laser data. First, binary crack maps are divided into sub-blocks. Second, sub-blocks are classified and the regions of confidence (ROC) are selected. Third, ROCs are filtered by checking the direction coherence. At last, the minimum cost spanning tree is adopted to extract the final cracks.

A. Crack sub-block classification

The binary map is divided into sub-blocks, e.g., 20×20 pixels, for initialization and rapid extraction of the crack region. After that, a classification method based on SVM is used to classify the sub-blocks, and the sub-blocks that are likely to contain cracks are selected on the binary crack map, which are called *crack sub-blocks*.
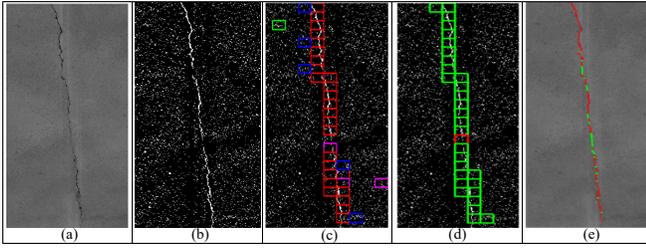
Fig. 3. An illustration of pavement crack detection. (a) A laser range image produced from frequency band-pass filtering. (b) The binary map of potential cracks. (c) SVM classification of sub-blocks. (d) Crack sub-blocks filtering and linking. (e) Target-point growing.
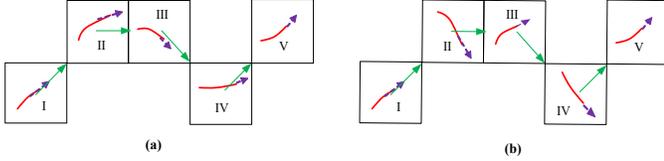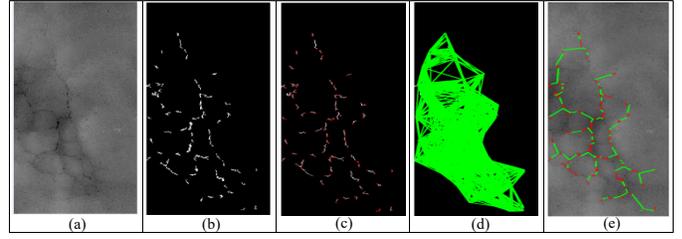

Fig. 5. An illustration of crack seeds grouping. (a) A pavement depth map. (b) The crack seed regions. (c) The crack seed points (in red). (d) Crack seeds association. (e) Crack seeds grouping result.

Fig. 4. (a) A set of morphological sub-blocks with high confidence. (b) A set of morphological sub-blocks with low confidence.

B. Crack sub-blocks filtering

The crack sub-blocks can be regarded as a narrowed crack region. The crack geometry, cracking direction of extension and spatial aggregation are similar for the sub-blocks of a true crack. Considering that the cracks have a certain length, extension trend and aggregation in the cracking direction, the crack sub-blocks with low length, larger direction deviation and low degree of aggregation in the main direction hold lower confidence. Accordingly, the following rules are designed to filter the crack sub-blocks:

i) Crack-length filtering. The crack length refers to the sum of crack length of a sub-blocks set. The confidence of the sub-blocks set with short length is low. A threshold T_l is set to indicate the crack sub-blocks with high confidence.

ii) Direction-coherence filtering. The sub-blocks should have similar cracking properties. The sub-block direction can be determined by the spatial relationship between the current sub-block and the next sub-block, as illustrated by the solid-line arrows in Fig. 4. Comparing the direction a neighboring region (θ_{nei}) and the direction of the current sub-block direction (θ_{cur}), if $|\theta_{nei} - \theta_{cur}| < T_\theta$, they are considered as consistent, where $T_\theta = \pi/4$. Figure 4 illustrates the above filtering settings.

iii) Crack sub-blocks linking. A pavement crack is typically an irregular linear target, which is formed by short crack segments, and influenced by the road conditions. In the range image, the depth values of shallow segments of a crack are small. These shallow crack segments usually lead to the two complications: (i) true crack sub-blocks may be classified as non-crack sub-blocks; (ii) crack sub-blocks may be judged as noise sub-block and removed in the filtering process. Thus, cracks often break at the shallow crack segments. In this paper, sub-blocks with similar spatial location and direction

are linked as a whole, which ensures that the sub-block sets exactly cover the area where the cracks are located and facilitates the complete detection of cracks.

- Calculating the sub-block set's direction θ;
- Collecting the endpoint set of the sub-blocks E;
- Calculating the minimum Euclidean distance $minD_{ij}$ between endpoint set E_i and E_j. If $minD_{ij} < T_d$, and $|\theta_{nei} - \theta_{cur}| < T_\theta$, the crack sub-blocks satisfy the extension condition and should be linked.

A real example for crack sub-blocks filtering and linking is shown in Fig. 3(d).

C. Crack seeds grouping

A target-points grouping algorithm based on the minimum cost spanning tree is presented to complete the crack extraction. It contains the following steps:

i) Extracting the original crack seed region. Firstly, the potential crack points with longer connection length in the sub-block region are extracted as the original crack seed region, and the connection length threshold T_{sc} is defined by Eq. 5, where L_{sc} is the length of current sub-blocks set.

$$T_{sc} = min(100, max(30, 0.05 * L_{sc}))$$ (5)

ii) Selecting crack seeds. In order to get the endpoint and the crack direction of the seed region accurately, the seed region should be refined to get the crack skeleton in it. The corner detection method is used to extract the turning points of the crack skeleton, which will serve the adaptive partitioning the crack skeleton into short segments. The endpoints of crack segments are taken as the crack seeds.

iii) Associating crack seeds. Two pairs of cracked seed points are connected, if the two seed points belong to the same crack seed region, the edge is replaced by the crack segment itself, and marked as the real edge. Otherwise, it is marked as the virtual edge. Where the set of real edges is denoted by $\mathcal{R}$ and the set of virtual edges is denoted by $\mathcal{V}$.

iv) Assigning weight values to the edges. The value and confidence of the edge are positively correlated – the lower confidence, the smaller the edge weight. In addition, according to the geometric characteristics such as the length and direction of the real edge, we assign the weight to the real edge, and then take the real edge weight as the reference and assign each virtual edge a reasonable weight by considering the grouping
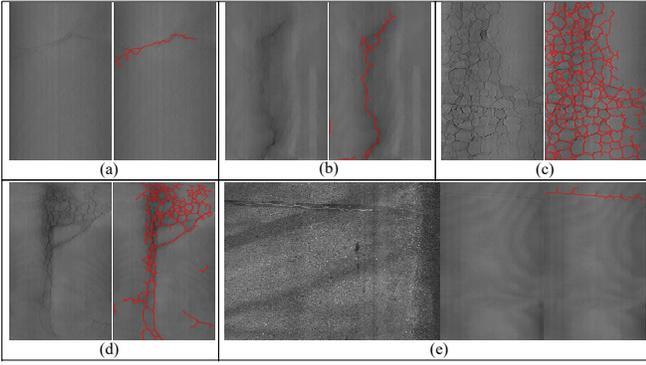
Fig. 6. Experimental results on different types of cracks. (a) Traverse crack. (b) Longitudinal Crack. (c) Block crack. (d) Irregular crack. (e) Repaired crack. Note that, an optic image is provided in the left of (e) to show the repaired crack.

rule of proximity, similarity and continuity. Specifically, the weight value is calculated by Eq. 6.

$$\mathcal{W}_{i,j} = \begin{cases} 0.1, \ if \ e_{i,j} \in \mathcal{R} \\ l_{i,j}, \ else \ if \ e_{i,j} \in \mathcal{V}, l_{i,j} \leqslant T_L \\ l_{i,j} + l_{i,j} * (\mathcal{C}'_{i,m_i} + \mathcal{C}'_{j,m_j}) * |\theta_{i,m_i} - \theta_{j,m_j}|/\pi, \\ \quad else \ if \ e_{i,j} \in \mathcal{V}, l_{i,j} > T_L, e_{m_i,i}, e_{m_j,j} \in \mathcal{R} \end{cases}$$

$$\tag{6}$$

where

$$\mathcal{C}_{i,j} = \frac{1}{0.5 * l_{i,j}/L_{max} + 0.5 * Ol_{i,j}/OL_{max}}, \ if \ e_{i,j} \in \mathcal{R} \tag{7}$$

and

$$\mathcal{C}'_{i,j} = C_{i,j}/SR_{max}, \ if \ e_{i,j} \in \mathcal{R}. \tag{8}$$

In the above formulations, i, j denote the index of a pair of crack seeds, $e_{i,j}$ denotes the edge with seeds i and j being its two vertex. $l_{i,j}$ denotes the length of $e_{i,j}$. $C_{i,j}$ and $C'_{i,j}$ denote the original weight and the normalized weight of $e_{i,j}$, respectively. $Ol_{i,j}$ is the length of the original crack seed region of edge $e_{i,j}$. L_{max} and OL_{max} are the maximum length values of the edges and the original crack seed regions, respectively. SR_{max} is the maximum original weight, $\theta_{i,j}$ represents the direction from the seed point i to the seed point j. As for m_i and m_j, they denote the indices of the corresponding points which are at the other side of i and j in the real edges.

v) Crack seeds grouping. The crack path is obtained by using the principle of minimum cost spanning tree, and the crack path is fused with the crack seed region. After that, the final cracks is obtained. Figure 5(e) shows an example result of crack seeds grouping. In Fig. 5(d), only the edges with lower weights are plotted in order to make a clear display. The red color in Fig. 5(e) indicates the crack seed region while the green color indicates the crack linking.

IV. EXPERIMENTS AND RESULTS

In order to validate the effectiveness and verify the universality of the proposed method, a large number of real collection laser profiling data are used for evaluation, which includes different types of cracks captured at different traffic speeds.

The data included five types of cracks: traverse crack, longitudinal crack, block crack, irregular crack and repaired crack. Some results are shown in Fig. 6, where the crack detection results are marked with red lines. Note that, in Fig. 6(e), the leaded oil makes no significant depth change in the range image.

To quantitatively illustrate the accuracy of the proposed method in detecting various types of cracks, 13.3 thousand data samples captured in 10 road sections are used for evaluation. The results are listed in Table I. Note that, **P** denotes the number of images containing cracks, **N** denotes the number of images without cracks. **FN** denotes the number of the images judged as non-cracked images but indeed containing cracks. **FP** denotes the number of the images judged as cracked images but indeed not containing cracks, **TP** denotes the number of images in which cracks are correctly identified, and **TN** denotes the number of non-cracked images that are correctly identified. In this paper, three metrics **FNR** (false negative rate), **FPR** (False Positive Rate) and **PPR** (Predicted Positive Rate), which are defined by Eq. 9, are used to evaluate the crack detection performance.

$$\begin{cases} \mathbf{FNR} = \mathbf{FN}/\mathbf{P} * 100\% \\ \mathbf{FPR} = \mathbf{FP}/(\mathbf{TP} + \mathbf{FP}) * 100\% \\ \mathbf{PPR} = (\mathbf{TP} + \mathbf{TN})/(\mathbf{P} + \mathbf{N}) * 100\% \end{cases} \tag{9}$$

TABLE I
RESULTS ON A LARGE-SCALE DATASET.

Crack Type	Crack Width (mm)	N	P	TP	TN	FN	FP	FNR (%)	FPR (%)	PPR (%)
Traverse Crack	$\leqslant 2$	186	13396	132	13333	54	63	29.0	32.3	99.1
	$\geqslant 2$	736	12846	689	12778	47	68	6.4	9.0	99.2
Longit. Crack	$\leqslant 2$	157	13425	133	13396	24	29	15.3	17.9	99.6
	$\geqslant 2$	468	13114	441	13078	27	36	5.8	7.5	99.5
Block Crack	$\leqslant 3$	157	13425	145	13408	12	17	7.6	10.5	99.8
	$\geqslant 3$	831	12751	811	12715	20	36	2.4	4.3	99.6
Irregular Crack	$\leqslant 3$	131	13451	118	13425	13	26	9.9	18.1	99.7
	$\geqslant 3$	821	12761	812	12739	9	22	1.1	2.6	99.8
Repaired crack	–	872	12710	852	12687	20	23	2.3	2.6	99.7

It can be observed from Table I that, the overall detection rate of all types of cracks in the experiments is above 98.0%. Under the same conditions, the wider the crack width, the lower the **FNR** and the **FPR**. This is because that wider cracks have better continuity on the pavement. The **FNR** and **FPR** of the block cracks and the irregular cracks are lower than that of the traverse and longitudinal cracks. The possible reason is that most of the crack width of a block crack or an irregular crack are generally wider than that of the traverse and longitudinal cracks. The identification accuracy of longitudinal crack is higher than that of traverse crack. The main reason for this phenomenon is that the resolution of the laser imaging data in the longitudinal direction is higher than that in the traverse direction. The above results show that

proposed method obtains accurate and complete detection of five different types of pavement cracks on the laser imaging profiling data.

In order to examine the effect of speed on the performance of the proposed method, various traffic speeds, i.e., 10, 20, 30, 40, 50, 60, 70 and 80 km/h, are used when measuring the same road section. A sample pair of captured laser range images and the crack detection results at 30km/h and 80km/h are shown in Fig. 7. It can be seen from Fig. 7, the detected cracks are similar for the two speed settings, which demonstrates the method proposed in this paper can meet the requirement of detecting the crack at different measuring speeds. Meanwhile, with the increase of measuring speed, the posture turbulence of the vehicle becomes more and more heavy. However, the crack detection results are also very good when suffering from heavy posture turbulence in high speed measurement. The main reason is that this method can eliminate the influence of posture turbulence by extracting the potential crack points in data pre-processing by separating the pavement control profile from the laser profiling section data.

In addition, comparisons are conducted by applying the proposed method on optic images and laser range images with regarding to the same road areas. Several example image pairs and crack detection results are shown in Fig. 8. We can see, the optic imaging can easily be influence by illuminance variation, and the cracks in the laser range images are more apparent than in optic images, and the crack detection results on laser range images are better, which indicates that the proposed crack detection method using 3D laser imaging has a good applicability for measuring under ambient illumination.
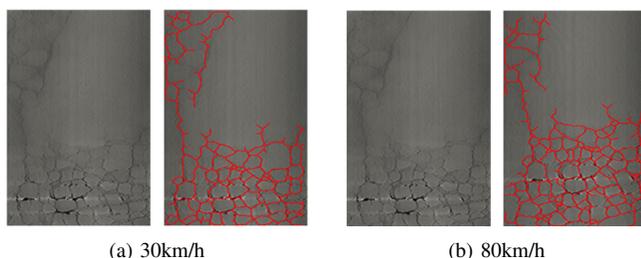

(a) 30km/h   (b) 80km/h

Fig. 7. Crack detection results at different speeds.

V. Conclusion

In this paper, pavement crack detection using 3D laser profiling data was studied. The frequency analysis was performed to decompose the profiling data, and potential crack map was generated. Then a sparse points grouping method was proposed to detect the cracks from the binary crack map. Experiments on a large laser profiling dataset showed that the proposed method can effectively detect different types of cracks such as the traverse crack, longitudinal crack, block crack, irregular crack and repaired crack at different measuring speeds. Compared with the optic-imaging-based crack detection method, the 3D laser crack detection method can overcome the influence of cast shadow and uneven illumination.
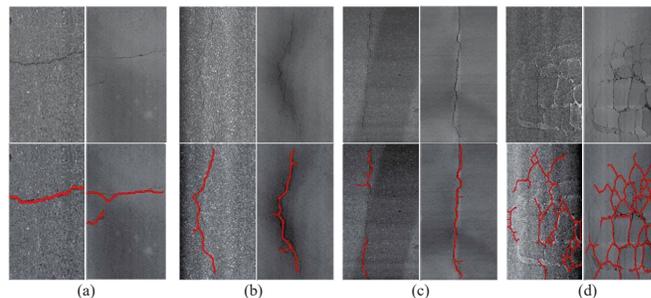

Fig. 8. Comparison of crack detection results on 2D and 3D pavement data.

References

[1] H. Oliveira and P. L. Correia, "Automatic road crack segmentation using entropy and image dynamic thresholding," in *European Signal Processing Conference*, 2009, pp. 622–626.

[2] Q. Zou, Y. Cao, Q. Li, Q. Mao, and S. Wang, "CrackTree: Automatic crack detection from pavement images," *Pattern Recognition Letters*, vol. 33, no. 3, pp. 227–238, 2012.

[3] H. Oliveira, J. Caeiro, and P. L. Correia, "Accelerated unsupervised filtering for the smoothing of road pavement surface imagery," in *European Signal Processing Conference*, 2014.

[4] H. Oliveira and P. Correia, "Automatic road crack detection and characterization," *IEEE Transactions on Intelligent Transportation Systems*, vol. 14, no. 1, pp. 155–168, 2013.

[5] M. Avila, S. Begot, F. Duculty, and T. S. Nguyen, "2D image based road pavement crack detection by calculating minimal paths and dynamic programming," in *IEEE Conference on Image Processing (ICIP)*, 2014.

[6] R. Amhaz, S. Chambon, J. Idier, and V. Baltazart, "Automatic crack detection on two-dimensional pavement images: An algorithm based on minimal path selection," *IEEE Transactions on Intelligent Transportation Systems*, vol. 17, no. 10, pp. 2718–2729, 2016.

[7] D. Zhang, Q. Li, Y. Chen, M. Cao, L. He, and B. Zhang, "An efficient and reliable coarse-to-fine approach for asphalt pavement crack detection," *Image and Vision Computing*, vol. 57, pp. 130–146, 2017.

[8] Q. Zou, Z. Hu, L. Chen, Q. Wang, and Q. Li, "Geodesic-based pavement shadow removal revisited," in *IEEE International Conference on Acoustics, Speech and Signal Processing*, 2016, pp. 1761–1765.

[9] J. Laurent, D. Lefebvre, and E. Samson, "Development of a new 3D transverse laser profiling system for the automatic measurement of road cracks," in *6th Symposium on Pavement Surface Characteristics*, 2008.

[10] Y.-C. Tsai and F. Li, "Critical assessment of detecting asphalt pavement cracks under different lighting and low intensity contrast conditions using emerging 3d laser technology," *Journal of Transportation Engineering*, vol. 138, no. 5, pp. 649–656, 2012.

[11] W. Ouyang and B. Xu, "Pavement cracking measurements using 3D laser-scan images," *Measurement Science and Technology*, vol. 24, no. 10, 2013.

[12] R. Medina, J. Llamas, E. Zalama, and J. Gomez-Garcia-Bermejo, "Enhanced automatic detection of road surface cracks by combining 2D/3D image processing techniques," in *IEEE International Conference on Image Processing (ICIP)*, 2014, pp. 778–782.

[13] C. Jiang and Y. J. Tsai, "Enhanced crack segmentation algorithm using 3D pavement data," *Journal of Computing in Civil Engineering*, vol. 30, no. 3, pp. 1–10, 2015.

[14] Q. Zou, Q. Li, F. Zhang, Z. Xiong, and Q. Wang, "Path voting based pavement crack detection from laser range images," in *IEEE Conference on Digital Signal Processing(DSP)*, 2016, pp. 432–436.

[15] A. Zhang, K. C. Wang, R. Ji, and Q. J. Li, "Efficient system of cracking-detection algorithms with 1-mm 3D-surface models and performance measures," *Journal of Computing in Civil Engineering*, vol. 30, no. 6, p. 04016020, 2016.